

A Comparative Attention Framework for Better Few-Shot Object Detection on Aerial Images

Pierre Le Jeune and Anissa Mokraoui

Abstract—Few-Shot Object Detection (FSOD) methods are mainly designed and evaluated on natural image datasets such as Pascal VOC and MS COCO. However, it is not clear whether the best methods for natural images are also the best for aerial images. Furthermore, direct comparison of performance between FSOD methods is difficult due to the wide variety of detection frameworks and training strategies. Therefore, we propose a benchmarking framework that provides a flexible environment to implement and compare attention-based FSOD methods. The proposed framework focuses on attention mechanisms and is divided into three modules: spatial alignment, global attention, and fusion layer. To remain competitive with existing methods, which often leverage complex training, we propose new augmentation techniques designed for object detection. Using this framework, several FSOD methods are reimplemented and compared. This comparison highlights two distinct performance regimes on aerial and natural images: FSOD performs worse on aerial images. Our experiments suggest that small objects, which are harder to detect in the few-shot setting, account for the poor performance. Finally, we develop a novel multiscale alignment method, Cross-Scales Query-Support Alignment (XQSA) for FSOD, to improve the detection of small objects. XQSA outperforms the state-of-the-art significantly on DOTA and DIOR.

Index Terms—Few-Shot Learning, Object Detection, Aerial Images, Attention, Small Objects.



1 INTRODUCTION

IMPRESSIVE progress has been made in object detection in the past decade, mostly because of deep convolutional networks (see e.g. [1], [2]). Current state-of-the-art performs high-quality object detection, but it requires large annotated datasets and days of training to achieve such quality. Often, these requirements could not be met, and it is quite hard to achieve good performance for a specific application. Few-shot learning focuses specifically on this kind of use cases where data is scarce. It has been extensively studied for classification in the past years. However, detection is a more challenging task and has been only tackled recently from a few-shot perspective.

Few-Shot Object Detection (FSOD) is a challenging problem that aims to find all occurrences of a class in an image given only a few examples. Current FSOD state-of-the-art is mainly based on attention mechanisms, which aim at extracting information about the task (i.e. semantic features about the classes to be detected) from *support* examples. Hence, the network can condition the detection on the examples. A seminal work in this direction is presented in reference [3] which reweights features from the input image (also called *query* image) with the features extracted from the support images. Plenty of methods based on the same idea have since been introduced (see e.g. [4], [5], [6], [7]). Although the attention mechanisms proposed in these papers differ from the original one, the main principle remains the same. It combines information from the query image and the support examples to detect only the objects annotated in the support set.

The FSOD field is rapidly growing, and most new papers propose a novel attention technique. However, there are a

lot of design choices that can be considered to address the FSOD problem. The detection framework and its backbone, the loss function and all the hyperparameters that are tied to these methods make the comparison between FSOD methods difficult. This paper focuses first on filling this shortcoming. To do so, we propose a modular attention framework that regroups most attention-based methods under the same notations. Specifically, this framework is divided into three parts: spatial alignment, global attention, and fusion layer. This separation helps to easily implement the different mechanisms and facilitates the comparison. Most importantly, this makes it possible to completely fix the other parameters and design choices without reimplementing each method from scratch. That way, a fair comparison of different attention mechanisms is possible. To help the development of future FSOD comparisons, the code of the proposed framework is available¹. Some FSOD methods are selected and reimplemented inside the framework to demonstrate its efficacy. Most of these methods have originally been tested on Pascal VOC [8] and MS COCO [9]. However, when it comes to others datasets, specifically aerial images, there lacks comparative studies about FSOD. Therefore, we propose a comparison of several competitive FSOD methods on two aerial datasets: DOTA [10] and DIOR [11]. It appears that FSOD methods perform poorly on aerial images, in comparison with classical detection (i.e. without few-shot). We hypothesize that this is due to a greater proportion of small objects in aerial images. They are notoriously hard to detect, even when plenty of examples are available. In FSOD, it is even more difficult. Not only the model needs to detect small objects, but also it needs to figure out what class to detect from small examples. It makes the small FSOD much harder than small objects detection

- Pierre Le Jeune is with L2TI, Université Sorbonne Paris Nord and COSE.
- Anissa Mokraoui is with L2TI, Université Sorbonne Paris Nord.
- Corresponding E-mail: pierre.le-jeune@cose.fr

1. https://github.com/pierlj/aaf_framework

as the error can also come from the conditioning of the network. Empirical results supporting this hypothesis are presented in this work. To alleviate this issue, a new attention based FSOD method is proposed. It computes attention between different feature levels, enabling a stronger query-support matching. This novel method performs better than existing methods on small objects and outperforms state-of-the-art on DOTA and DIOR.

The contributions of this paper are summarized as follows:

- 1) A review of existing works for FSOD with a focus on attention-based methods.
- 2) A generic and modular structure, named Alignment, Attention, Fusion (AAF) framework is designed to implement and compare existing attention mechanisms for FSOD.
- 3) A comparative performance study based on Relative Mean Average Precision (RmAP), a proposed metric for FSOD methods, and an analysis of the specific difficulties of applying FSOD on aerial images.
- 4) A novel multiscale attention method, named Cross-Scales Query-Support Alignment (XQSA) for FSOD, specifically designed for small objects. It outperforms previous techniques on aerial images, but also on natural images to a lesser extent.

2 REVIEW OF EXISTING WORK ON FSOD

This section first presents a brief summary of object detection and few-shot learning. Then, a thorough review of few-shot object detection is conducted, focusing especially on attention-based methods.

2.1 Object Detection

Object detection has made impressive progress with the rise of Convolutional Neural Networks (CNN). YOLO [2] and Faster R-CNN [1] have been the first fully convolutional approaches for object detection. These two architectures are the most representative examples of the two kinds of detectors that exist: one-stage and two-stages detectors. Plenty of improvements have been introduced over these methods. Focal Loss [12] improves training balance between background and foreground objects. Fully Convolutional One-Stage object detection (FCOS) [13] gets away from the concept of anchors boxes. Feature Pyramid Network (FPN) [14] improves detection of objects of various sizes. Recently, various works exploit self-attention mechanisms to increase detection quality. Dynamic Head [15] combines three different types of attention, based on scale, location and current task. Pushing even further, DETR [16] replaces the convolutional regressor and classifier with transformers.

2.2 Basic Concepts on Few-Shot Learning

Few-Shot Learning (FSL) aims at learning tasks from only limited data. The main principle is to first learn generic knowledge and then adapt the model based on the limited data available. Generally, the adaptation phase consists in adding new classes (novel classes) to the problem. We talk about K -shots, N -ways learning when only K examples are available for each of the N novel classes. For a given dataset, it is common to divide the set of classes into base and

novel classes. Base classes are used during training while novel classes are reserved to assess the generalization capabilities of the models. There exist different approaches for FSL, we propose a classification of these methods into four categories: fine-tuning, meta-learning, metric learning and attention-based. This classification is designed for FSOD and our analysis, but a more complete taxonomy has already been proposed by [17].

Fine-tuning – It consists in training the model on a large dataset with base classes examples only and then fine-tune it with a few examples for the novel classes. While conceptually simple, these approaches are often prone to catastrophic forgetting [18]: performance drops on base classes after fine-tuning. Fine-tuning on its own is not very powerful for FSL, but it is part of most other methods as their training strategy.

Meta-learning – It attempts to learn models that can quickly adapt to a task. This is often achieved through an *episodic training strategy*. To mimic FSL testing conditions, at each episode, a subset of classes $\mathcal{C}_{ep} \subset \mathcal{C}$ is sampled, along with a few examples divided into support and query sets, containing objects from \mathcal{C}_{ep} . The model is trained on the query set and has access to supplementary information in the support set. This can be leveraged to choose an initialization point [19] or to perform weight updates [20]. While the latter methods require the use of an auxiliary network and therefore do not scale very well, the episodic strategy helps to train adaptive models and is employed in many other FSL methods.

Metric Learning – This has been introduced for FSL by Prototypical Networks [21]. It aims at learning an embedding function from the base dataset, such that the embedding space is semantically structured. Input images are then classified according to the distance between their representations and the representations of the support examples.

Attention-based FSL – It uses support representations to change the parameters of the model and adapt to new tasks on the fly. Reference [22] proposes a *learnnet* whose purpose is to output weights for the main network based on the support images. Hence, the network has dynamic convolutional filters and can adapt to new classes. This can be seen as an attention mechanism between a query image and support images: the query features are reweighted by the support features through a channel-wise multiplication. Attention is meant to highlight features that are relevant for the task. In the case of self-attention, this can be achieved by channel multiplication with the map itself, as proposed by [23]. It can also be with spatially distant features of the same image as in non-local neural networks [24] or Visual Transformers (ViT) [25]. But attention can also be computed with features coming from different images. This can be used for FSL to highlight support features in query features. For instance, Cross-Transformers [26], leverage a transformer-like attention to align support and query features.

2.3 Few-Shot Object Detection

This section aims at reviewing the FSOD literature. While more emphasis is put on attention-based methods, it also presents works from other few-shot areas: fine-tuning, metric learning and meta-learning. Few methods rely solely on meta-learning, these are included in other subsections.

TABLE 1

Comparison of the FSOD methods from an attention perspective. This table separates the attention mechanisms into three components: spatial alignment, global attention, and fusion layer. All frameworks are working with multiscale features except for the one with the mention no FPN. For fusion layer, concatenation is denoted as $[\cdot, \cdot]$, while other pointwise operations are represented by a circle operator (e.g. \oplus for addition). Learnable modules are denoted by $\dagger\dagger$.

Approach	Name	Date	Framework	Alignment	Global Attention	Fusion
Attention	FRW [3]	2019	YOLO (no FPN)	None	GP + CRW	None
	RSI [4]	2019	YOLO	None	GP + CRW	None
	MRCNN [27]	2019	Faster R-CNN (no FPN)	None	GP + CRW	None
	ARMRD [28]	2020	Faster R-CNN	None	GP + CRW	None
	VEOW [29]	2020	Faster R-CNN	None	GP + CRW	Pool + $[\odot, \ominus, Id]$
	WSAAN [30]	2020	Faster R-CNN	None	GP + GNN + CRW	None
	CACE [6]	2020	Faster R-CNN	QS Alignment	GP + CRW	None
	KT [31]	2020	Faster R-CNN	None	GP + GNN + CRW	None
	IFSOD [32]	2021	Center Ne (no FPN)	None	GP + GNN + CRW	None
	WOFT [7]	2021	FCOS	None	GP + CRW	Pool + $[\cdot, \cdot]^{\dagger\dagger}$
	FPDI [33]	2021	Faster R-CNN	Iterative Alignment via Optimization	CRW	None
	MFRCN [34]	2021	Faster R-CNN	RoI Pooling + QS Alignment	Global Similarity RW	$[\ominus, [\cdot, \cdot]]^{\dagger\dagger}$
	MDETR [35]	2021	DETR (no FPN)	Transformers-based Alignment	Transformers Self-Attention	None
	DRL [36]	2021	Faster R-CNN	None	None	Pool + $[\odot, \ominus, Id]$
	DANA [37]	2021	Faster R-CNN and RetinaNet	QS Alignment	Background Attenuation	$[\cdot, \cdot]$
	SP [38]	2021	Faster R-CNN	Self-Alignment (query and support)	None	$[\cdot, \cdot]$
	JCACR [39]	2021	YOLO	QS Alignment (higher order)	None	$[\cdot, \cdot]$
	TI [40]	2021	Faster R-CNN	None	None	$[\cdot, \cdot]$
	FCT [41]	2022	Faster R-CNN	QS Alignment (with fused keys)	None	$[\cdot, \cdot]$
	Attention/ Metric	PNPDet [42]	2021	Center Net (no FPN)	None	CRW
UPE [43]		2021	Faster R-CNN	QS Alignment	None	$Id \oplus [\cdot, \cdot]^{\dagger\dagger}$
GD [44]		2021	FCOS	None	GP + CRW	None
Metric Learning	RM [45]	2018	Faster R-CNN	None	None	None
	RNI [46]	2020	Faster R-CNN	None	None	None
	FSCE [47]	2021	Faster R-CNN	None	None	None
	PFRCN [48]	2021	Faster R-CNN	None	None	None
	AD [49]	2021	Faster R-CNN	None	None	None
	GDSVD [50]	2021	Faster R-CNN	None	None	None
Fine- tuning	LSTD [51]	2018	Faster R-CNN	None	None	None
	WOFG [52]	2020	Faster R-CNN	None	None	None
	TFA [53]	2020	Faster R-CNN	None	None	None
	MSPSR [54]	2021	Faster R-CNN	None	None	None
	DETRG [55]	2021	Faster R-CNN	None	None	None
	HFSOD [56]	2021	Faster R-CNN	None	None	None
	DHP [57]	2021	Faster R-CNN	None	None	None
	SAM [58]	2021	Faster R-CNN	None	Channel + Spatial Attention	None
	SIMPL [59]	2021	Faster R-CNN (no FPN)	None	None	None

2.3.1 Fine-tuning

Low Shot Transfer Detector (LSTD) is a pioneer work on FSOD [51]. It proposes to first train a detector on a base dataset and fine-tune it on a novel set containing only some examples of the novel classes. Regularization losses are introduced to prevent catastrophic forgetting. Closely related, reference [53] leverages the same idea without additional loss. Instead, they freeze most of the network after base training. Reference [54] also proposes a basic fine-tuning strategy by leveraging a multiscale refinement branch. It provides a better balance between positive and negative samples and makes both base training and fine-tuning more efficient. Another proposed method [52] trains two Faster R-CNN: one on base classes and one on all classes (base and novel), as a fine-tuned version of the first one. Outputs from both detectors are combined at test time to achieve better performance on base and novel classes.

2.3.2 Metric Learning

Metric-learning based methods are extensively employed for few-shot classification. For detection however, it remains unusual and therefore neglects object localization. RepMet [45] learns class representative vectors to classify Regions of Interest (RoI) in Faster R-CNN. Closely related, [42] learns prototype vectors as well as scale factors. This differs slightly from the original metric learning paradigm as

prototypes are learned through training and not computed from examples like in Prototypical Faster R-CNN [48]. The authors of this method propose to replace the classification layers in both stage of Faster R-CNN by prototypical networks. Similarly, FSCE [47] computes the prototypes directly from the examples but only in the second stage of the network. In addition, it leverages a contrastive loss function to better organize the embedding space. Reference [43] also uses prototypes, but as reweighting vectors to enhance class-specific features of the embedded RoI.

2.3.3 Attention-based

The main principle of attention-based FSOD is to highlight relevant features for detection of a particular class, based on examples of that class. A seminal work in this field is [3], which trains a reweighting module along with a YOLO detector. The reweighting module produces class-specific feature vectors with a Global Pooling (GP) on the support feature maps. These are then channel-wise multiplied with the query features extracted by the backbone. Hence, class-specific query features are generated, and the detection head computes predictions for each class separately. We denote this operation as Class Re-Weighting (CRW). This has been used with different detection frameworks, for instance, references [7] and [29] are built upon Faster R-CNN and FCOS respectively. Other authors proposed to leverage multiscale reweighting vectors, such as in [4] for an application on

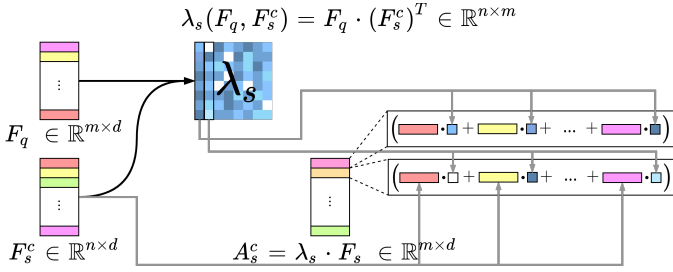


Fig. 1. Spatial alignment between query and support feature maps. Similarity matrix is based on outer product between the maps. For sake of clarity, maps are reshaped as 2-D matrix where the first dimension controls the spatial position in the map: m positions for the query and n for the support. d is the number of channels. Similar colors mean that features are similar.

aerial images. More sophisticated ways to combine information from query and support have also been proposed. For instance, reference [28] trains three different heads that link, globally, locally, and patch-to-patch, the features from the query and the support. Graph Neural Networks (GNN) can also combine the features and learn semantic relations between classes (see e.g. [30], [31]). Another way to combine query and support is to concatenate the features as in [15].

The attention-based methods presented above are *global*. The features of a support example are compressed into a single vector and spatial information is lost. To prevent this, spatial attention is introduced in several methods. It can be seen as a spatial realignment of the features. For each location in the query map, the features from a support example are linearly combined according to a chosen similarity measure (see Fig. 1). This highlights common features between query and support images while preserving spatial information. We will refer to this as Query-Support Alignment (QSA) in the following. This kind of alignment has been introduced in [24] for video classification. References [37], [39] are based on this approach. Thus, the aligned maps can be easily combined and fed to the detection head. The combination is often performed through a fusion layer composed of several point-wise operations. In some cases, additional learnable modules are included to process the combination of query and support features before fusion, this is indicated with the symbol $\dagger\dagger$ in Tab. 1. The alignment mechanism can be associated with the global attention methods mentioned in the previous paragraph as in [6] and [34]. Alignment can also be carried out on the feature itself (i.e. without information from the support) as in [35], [38]. This self-alignment (or self-attention) is at the heart of transformers. DETR [16] is a detection framework based on ViT. It is therefore well suited for this kind of alignment mechanisms. The few-shot variant of DETR, Meta-DETR described in [35], combines both self-attention and query-support alignment, achieving impressive performance.

Tab. 1 summarizes this literature analysis. Attention mechanisms are split into the three components that were highlighted in Sec. 2.3.3: spatial alignment, global attention and fusion layer. The table also includes FSOD methods described in previous sections that do not rely on an attention mechanism.

3 AAF FRAMEWORK FOR ATTENTION IN FSOD

In Sec. 2.3.3, three main components of attention mechanisms for FSOD have been identified: spatial alignment, global attention and fusion layer. Most attention-based FSOD methods rely on one or more of these components as shown in Tab. 1. To compare them fairly, we propose the Alignment, Attention and Fusion (AAF) framework. The purpose of this framework is to provide a flexible environment to implement attention-based FSOD methods. It takes as input the features from the query image F_q as well as the features extracted from every support images F_s^c for $c \in \mathcal{C}$ (the set of all classes). It outputs class-specific query features I_q^c in which features relative to class c are reinforced. To match the three components of attention described above, the framework is also divided into three parts as shown in Fig. 2. Each component is described below independently with examples of possible design choices. Even though this framework is presented from the perspective of object detection, it could be applied for any kind of few-shot tasks.

3.1 Query-Support Alignment

The alignment module, denoted Λ , spatially aligns the features from the query and the support. It is unlikely that objects of the same class appear at the same position inside query and support images. This issue is commonly avoided by pooling the support map and using it as a class-specific reweighting vector. But as discussed above, this trick loses the spatial information about the support object, which can be detrimental for detection. Instead, an alignment based on attention can be done between query and support feature maps. The idea is to re-organize one feature map in comparison with the other, so that similar features are spatially close in the maps. The alignment module is defined as follows:

$$\begin{aligned}
 A_q^c &= \lambda_q(F_q, F_s^c) F_q, & (1) \\
 A_s^c &= \lambda_s(F_q, F_s^c) F_s^c. & (2)
 \end{aligned}$$

Affinity matrices $\in \mathbb{R}^{n \times m}$ Support Features for class $c \in \mathbb{R}^{m \times d}$

The definition of the matrices λ_q and λ_s determines how features are aligned. This formulation is quite similar to the non-local blocks described in [24] and is at the heart of visual transformers [60]. Transformers attention can be understood as an alignment of the value to match the query-key similarity. This formulation allows implementing easily different feature alignments by changing the expression of the affinity matrices. As an example, Meta Faster R-CNN [34] leverages an alignment module with affinity matrices $\lambda_s(F_q, F_s^c) = F_q \cdot (F_s^c)^T$ and $\lambda_q(F_q, F_s^c) = I$ (see Example A in Fig. 2). Only the support features are aligned so that they match query features.

3.2 Global Attention

The global attention module, denoted Γ , combines global information of the supports and the query. It highlights

class-specific features and softens irrelevant information for the task. This module is defined as follows:

$$H_q^c = \gamma_q(A_q^c, A_s^c), \quad (3)$$

$$H_s^c = \gamma_s(A_q^c, A_s^c). \quad (4)$$

Highlighted features Global attention operators

The global attention operators γ_q, γ_s combine the global information from their inputs and highlight features accordingly. This is generally done through channel-wise multiplication. In this way, class-specific features are highlighted, while features not relevant to the class are softened. Changing the definition of γ_q and γ_s allows the implementation of a wide variety of global attention mechanisms. For instance, reference [3] pools the support maps with a global max pooling operation (GP) into a reweighting vector and reweights the query features channels with it: $\gamma_q(A_q^c, A_s^c) = A_q^c \otimes GP(A_s^c)$ and $\gamma_s(A_q^c, A_s^c) = A_s^c$ (see Example B in Fig. 2).

3.3 Fusion Layer

The purpose of the fusion component is to combine highlighted query and support maps. This is only applicable when the maps have the same spatial dimension. It is mostly used alongside with the alignment module as the latter does not combine the information from the support and the query but only reorganizes the maps. In particular, when support and query maps do not have the same spatial dimension, aligning support maps with query maps fixes the size discrepancy. The fusion module is defined as follows:

$$M_q^c = \Omega(H_q^c, H_s^c). \quad (5)$$

Merged query features Fusion operator

The highlighted maps can be combined through any point-wise operation, addition \oplus , multiplication \odot , subtraction \ominus , concatenation $[\cdot, \cdot]$ or more sophisticated ones. An example of such a fusion module is presented in [36]. The fusion operator concatenates the results of the addition and the subtraction of the highlighted features: $\Omega(H_q^c, H_s^c) = [H_q^c \oplus H_s^c, H_q^c \ominus H_s^c]$ (see Example C in Fig. 2). The point-wise operators can also contain small trainable models such as in [34], where small CNNs are applied after the point-wise operators, but before the concatenation: $\Omega(H_q^c, H_s^c) = [\psi_{dot}(H_q^c \odot H_s^c), \psi_{sub}(H_q^c \ominus H_s^c), \psi_{cat}([H_q^c, H_s^c])]$.

Except for the fusion layer which must be applied last, spatial alignment and global attention can be applied in any order. This flexibility is required to implement methods that apply global attention before alignment, such as DANA [37]. The author proposed a so-called background attenuation block that behaves like a self-attention block to refine support features. They applied it on support features before alignment. However, similar technique could very well be applied to query feature after alignment with support. Hence, the interchangeability is required to offer more flexibility to the framework. The whole architecture of the

AAF framework is illustrated in Fig. 2, in which examples from the previous sections are also depicted. The modular structure of the framework enables the implementation of a wide variety of attention mechanisms while keeping all other hyperparameters fixed. It is therefore a useful tool for FSOD methods comparison.

3.4 Implementation details

In order to make the comparison fair, some implementation details are kept fixed for all experiments. The backbone is a ResNet-50 with a 3-layers Feature Pyramid Network on top. It extracts features at 3 different levels, which helps the network to detect objects of various sizes. The detection head is based on FCOS [13]. Each feature level is processed by the same head to output detections of different sizes. The AAF framework is applied between the backbone and the detection head. As features are extracted at multiple levels, attention mechanisms are also implemented to work at different scales. This may differ from the original implementations, but most methods are already designed to work at multiscale (see Tab. 1). The networks are trained in an episodic manner. During each episode, a subset $\mathcal{C}_{ep} \subset \mathcal{C}$ of the classes is randomly sampled ($|\mathcal{C}_{ep}| = 3$). Only the annotations of the episode classes are used for training the model. A support set is sampled at each episode containing K examples for each episode class. A query set is also sampled for each episode, containing 100 images per class, hence 300 images are given to the model at each episode.

The training is divided in two phases *base training* and *fine-tuning*. During base training, only base classes can be sampled ($\mathcal{C}_{ep} \subset \mathcal{C}_{base}$) and one example per class is drawn for the support set ($K = 1$). The optimization is done with SGD and a learning rate of 1×10^{-3} for 1000 episodes. During *fine-tuning*, the backbone is frozen, the learning rate is divided by 10 and the episode classes can be sampled from $\mathcal{C}_{base} \cup \mathcal{C}_{novel}$, with at least one novel class per episode. Examples from novel classes are selected among the K examples sampled once before fine-tuning. Each model is fine-tuned separately for different value of $K \in 1, 3, 5, 10$. The base/novel class splits are selected randomly before training. 3 classes are selected as novel classes for DOTA, 5 for Pascal VOC and DIOR and 20 for MS COCO. The lists of the selected classes in our experiments are detailed in Appendix A. During both training phases, the same loss function is optimized, as defined in FCOS.

The evaluation is also conducted in an episodic manner, following recommendations from [61]. The performance is averaged over multiple episodes each containing 500 examples for each class and this is repeated multiple times with randomly sampled support sets. The query and support examples are drawn from test set, thus the support examples are different from the ones used during fine-tuning. This prevents overestimations of the performance due to overfitting on the support examples.

Some existing works leverage sophisticated training strategies (e.g. auxiliary loss functions [5], hard examples mining [56] or multiscale training [4]). While this certainly improves the quality of the detections, it introduces new parameters to tune and makes the comparison with other works difficult. As the focus of this study is about attention mechanisms, we chose not to reimplement all these

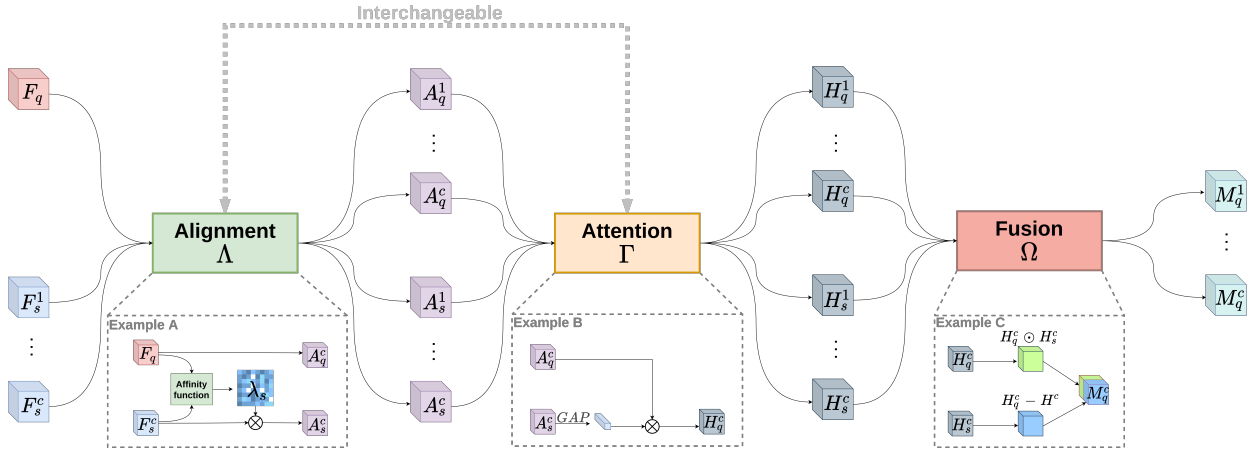


Fig. 2. The Alignment Attention Fusion (AAF) framework is composed of three components: spatial alignment Λ , global attention Γ and a fusion layer Ω . Examples for each module are depicted, these come from FSOD methods in the literature. Example A is presented in [34], Example B in [3] and Example C in [36]. The colors chosen in this diagram match the colors used in Equations (1) to (5).

improvements. However, to remain competitive with existing works, we propose a novel augmentation pipeline specifically designed for object detection. Its definition is described in Appendix B, which includes a cumulative study of its different components on DOTA. In addition, we chose the support extraction strategy among a few possibilities detailed in Appendix C. From our analysis, it seems that this design choice influences significantly the model performance (see Tab. 8). However, it is barely discussed in the FSOD literature. We find that the best strategy is to crop the support example and resize it to a fixed size patch. This strategy is thus fixed for all our experiments.

4 ATTENTION-BASED FSOD COMPARISON

To showcase the flexibility of the proposed AAF framework, we compare multiple existing works. Some methods described in Sec. 2 are selected: FRW [3], WSAAN [30], DANA [37], MFRCN [34] and DRL [36] (see Tab. 1). These have been chosen because they represent well the variety of attention mechanisms available in the literature. FRW is based on class-specific reweighting vectors, WSAAN has a more sophisticated global attention and computes reweighting vectors inside a graph structure. DANA and MFRCN leverage query-support alignment in different manners and DRL only uses a sophisticated fusion layer. Each of these methods has been reimplemented within the AAF framework. Of course, some details differ from the original implementations, but the purpose of this comparison is to compare only the attention mechanisms. In particular, the backbone and the training strategy (losses and episode tasks) may differ. We first conduct such a comparative experiment on Pascal VOC [8] and MS COCO [9] datasets. On these datasets, the performance achieved by our implementations is close to the values reported in the original papers (see Appendix D). Then, we use the framework to compare the performance of some methods on two aerial datasets: DOTA [10] and DIOR [11]. Finally, the following sections analyze the FSOD performance discrepancies on aerial and natural images.

4.1 Performance Analysis on Natural Images

First, compared to FCOS baseline on natural images, a slight performance drop on base classes is visible in Tab. 2 (FCOS achieves 0.66 mAP_{0.5} on Pascal VOC, all FCOS results are included in Tab. 11 in Appendix F). This is expected, even if the model has seen a lot of examples of these classes during training, its predictions are still conditioned on a few examples, which can sometimes be misleading. On the other hand, performance on novel classes is significantly lower than the FCOS baseline, especially for low numbers of shots. The number of shots is crucial for performance on novel classes. The higher the number of shots, the better the network performs. In average, with 10 examples per class, the network achieves 0.2 higher mAP than with 1 example. More examples provide more precise and robust class representations, improving the detection. The same phenomenon is observed with base classes to a lesser extent (+0.04 mAP from 1 to 10 shots). Fig. 10 in Appendix E displays these trends clearly, both for base and novel classes. In addition, Fig. 8 in the same appendix, provides the same results split by class.

The behavior just described is expected from any few-shot object detection method. Moreover, performance values are close to what is reported in the original papers of the reimplemented methods (see Tabs. 9 and 10 in Appendix D). These are not the exact same values as many architectural choices differ from the proposed methods (e.g. backbone, classes splits, etc.). Nevertheless, it confirms that the proposed AAF framework is flexible enough to implement a wide variety of attention mechanisms. It is therefore an appropriate tool to compare and design query-support attention mechanisms.

DRL is arguably the simplest method among the five selected as it leverages only a fusion layer. It combines query features with the features of each support image through concatenation and point-wise operations, creating class-specific query features. It is therefore the closest to the regular FCOS functioning. This explains the very good performance on base classes and lower mAP on novel classes, compared to the baseline. Regarding the other methods, FRW and WSAAN can be easily compared as both are based

TABLE 2

Performance comparison between five selected methods (see Sec. 4) on Pascal VOC. All are reimplemented with the proposed AAF framework. Mean average precision is reported for each method on base and novel classes separately and for various numbers of shots ($K \in \{1, 3, 5, 10\}$). For comparison, the FCOS baseline achieve 0.66 $mAP_{0.5}$ on Pascal VOC.

K	FRW [3]		WSAAN [30]		DANA [37]		MFRCN [34]		DRL [36]	
	Base	Novel	Base	Novel	Base	Novel	Base	Novel	Base	Novel
1	0.599	0.282	0.617	0.309	0.626	0.328	0.578	0.302	0.642	0.270
3	0.633	0.311	0.635	0.422	0.642	0.340	0.587	0.368	0.617	0.296
5	0.643	0.463	0.647	0.462	0.652	0.426	0.621	0.408	0.664	0.373
10	0.632	0.487	0.653	0.517	0.650	0.503	0.634	0.494	0.670	0.480

on global attention. The only difference is how the class-specific vectors are computed. In FRW, they are globally pooled from the support feature map. However, WSAAN combines the same vectors with query features in a graph. This certainly provides better class-specific features and in the end, better results both on base and novel sets. The remaining methods, DANA and MFRCN both leverage spatial alignment. While it seems to bring quite an improvement for DANA over FRW and DRL, the gain is smaller for MFRCN. In both methods, spatial alignment is not used alone. It is combined with other attention mechanisms. In DANA, a Background Attenuation block (i.e. a global self-attention mechanism) is applied to the support features to highlight class-relevant features and soften background ones. In MFRCN, aligned features are reweighted with global vectors computed from the similarity matrix between query and support features. This last operation may be redundant as the similarity information is already embedded into the aligned features, whereas background attenuation leverages new information.

From this comparison, one can conclude that both global attention and spatial alignment are beneficial for FSOD. However, these improvements may not always be compatible, as shown by the results of MFRCN. Hence, the design of each component must be done carefully so that spatial alignment, global attention, and fusion work in unison.

Another set of experiments is conducted on MS COCO dataset. Only the two best-performing methods on Pascal VOC are selected and trained on MS COCO following the same experimental setup. The results are summarized in Tab. 3. The mAP values are reported following standards from Pascal VOC ($mAP_{0.5}$ with one IoU threshold), and MS COCO ($mAP_{0.5:0.95}$ with several thresholds). MS COCO is a much more difficult detection benchmark, therefore the numbers of shots are adjusted: 1, 5, 10, and 30 shots. These results comfort the conclusion obtained on Pascal VOC: the framework is flexible enough to implement var-

TABLE 3

Performance comparison between WSAAN [30] and DANA [37] on MS COCO. $mAP_{0.5:0.95}$ (MS COCO mAP , with IoU thresholds ranging from 0.5 to 0.95) and $mAP_{0.5}$ values are reported for base and novel classes separately and for different numbers of shots: $K \in \{1, 5, 10, 30\}$.

K	WSAAN [30]				DANA [37]			
	$mAP_{0.5}$		$mAP_{0.5:0.95}$		$mAP_{0.5}$		$mAP_{0.5:0.95}$	
	Base	Novel	Base	Novel	Base	Novel	Base	Novel
1	0.335	0.120	0.201	0.066	0.355	0.145	0.213	0.078
5	0.399	0.199	0.236	0.105	0.428	0.222	0.252	0.119
10	0.409	0.214	0.244	0.115	0.430	0.237	0.256	0.129
30	0.415	0.222	0.247	0.121	0.435	0.244	0.260	0.133

ious FSOD techniques that achieve competitive results with state-of-the-art. As for Pascal VOC the models achieve better performance with more shots. Unlike Pascal VOC, base classes also benefit significantly from a larger number of examples on MS COCO. MS COCO being more difficult, the information extracted from the supports better helps the models. Finally, WSAAN outperforms DANA on Pascal VOC but performs slightly worse on MS COCO. It can be noted that, the results on a dataset cannot be extrapolated to another one. A method that performs best on a dataset is not guaranteed to do so on another dataset. This reinforces the need of a flexible framework that allows fair and easy comparison between FSOD methods. That way, the best performing method can be easily selected for a given problem.

From these experiments on natural images, it seems clear that DANA is the best performing method among the ones tested. Therefore, it highlights the importance of feature alignment for query-support matching. Global attention loses spatial information in support features which is detrimental for detection. However, global attention methods should not be overlooked. WSAAN shows impressive performance and even outperforms slightly DANA on Pascal VOC. It could be interesting to combine both methods, but this does not seem to be trivial as demonstrated by the results of MFRCN which basically leverages the alignment from DANA and the attention from FRW, but does not yield satisfactory results.

4.2 Performance Analysis on Aerial Images and comparison with natural images

To our knowledge, only three existing works evaluate FSOD methods on aerial images: FRW [29], WSAAN [4] and MFRCN [48]. All these methods are evaluated on different datasets, making their performance comparison difficult. Using the proposed AAF framework, we compare the performance of these methods both on DOTA and DIOR. These methods are reimplemented inside the framework and all common parameters are fixed during the experiments. In addition, DANA [37] is also included in the comparison as it was the best performing method on MS COCO. Tab. 4 regroups the results of these experiments. These results show a slight improvement over the state-of-the-art on DIOR (WSAAN [4]). Our implementation of WSAAN outperforms (0.08 mAP on base classes and 0.01 on novel classes) the result reported in the original paper. However, the attention mechanism employed in WSAAN is not optimal for aerial images. WSAAN is outperformed by both FRW and DANA. While this was expected for DANA in the light of results from Sec. 4.1, it was not for FRW.

TABLE 4

Comparison of $mAP_{0.5}$ of several methods on DOTA and DIOR datasets. For each method, mAP is reported for different number of shots $K \in \{1, 3, 5, 10\}$ and separately for base and novel classes. Blue and red values represent the best performance on base and novel classes respectively, for each dataset. Methods marked with a \dagger are not re-implemented in the AAF framework, their results are taken from the original papers. Our results in this table were published in a preliminary conference article [62], accepted at EUSIPCO 2022.

K	DOTA								DIOR									
	FRW		WSAAN		DANA		PFCRN \dagger		FRW		WSAAN		DANA		PFCRN \dagger		WSAAN \dagger	
	Base	Novel	Base	Novel	Base	Novel	Base	Novel	Base	Novel	Base	Novel	Base	Novel	Base	Novel	Base	Novel
1	0.47	0.13	0.46	0.12	0.49	0.13	0.29	0.08	0.57	0.17	0.56	0.16	0.59	0.21	0.41	0.06	-	-
3	0.47	0.25	0.44	0.24	0.50	0.21	0.34	0.10	0.58	0.25	0.52	0.14	0.59	0.27	0.40	0.08	-	-
5	0.49	0.30	0.48	0.31	0.53	0.25	0.32	0.09	0.61	0.33	0.61	0.30	0.62	0.34	0.42	0.09	-	0.25
10	0.49	0.37	0.47	0.35	0.53	0.34	0.35	0.11	0.62	0.36	0.62	0.33	0.62	0.36	0.42	0.09	0.54	0.32

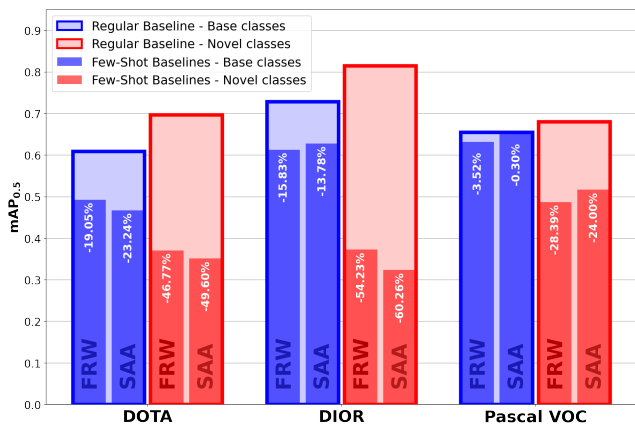


Fig. 3. Performance comparison between Regular Baseline and Few-Shot Baselines, FRW [4] and WSAAN (WSA) [30] on three datasets: DOTA, DIOR and Pascal VOC. On aerial image datasets, a large performance gap is observed on novel classes, while this is relatively reduced on Pascal VOC (i.e. natural images).

The superiority of DANA over the other methods on DOTA and DIOR is clear and coherent with the results on natural images. The more sophisticated attention mechanism, in particular the alignment, from DANA is better at extracting and leveraging the information from the support examples. Hence, the detection performance is higher. It is particularly beneficial for small number of shots: the extracted information is semantically robust.

However, it is surprising to see FRW performing so well, even better than DANA on DOTA’s novel classes. On Pascal VOC, which is similar to DOTA and DIOR in terms of size and number of classes, FRW performs largely worse than DANA. In addition to this inconsistency, another result is unsettling: the performance gap between the classical baseline (i.e. FCOS) and the few-shot approaches. On natural images, the performance drop is nearly inexistent for base classes and around 25% for novel classes. On aerial images these drops are largely increased: $\sim 15\%$ and $\sim 50\%$ for base and novel classes respectively. This can be guessed from Tabs. 2 and 4, but detailed gaps are provided in Fig. 3. Note that the FSOD baselines were trained here without augmentation, which explains slightly lower values than in tables from Secs. 4.1 and 4.2.

It seems tempting here to extrapolate the FSOD performance on DIOR from the performance on Pascal VOC. The classical baseline (FCOS) achieves similar performance on these two datasets, which contain the same number of classes and roughly the same number of images. There-

fore, one could have expected close FSOD performance on these datasets. This is quite different from the actual results reported in Fig. 3. It is generally irrelevant to compare the performance of a method from a dataset to another, especially with images of different nature. Each dataset has its own characteristics (resolution, intra-class variety, color range, etc.) and therefore a given model will not perform equally good on two distinct datasets with respect to a pre-defined performance metric. Hence, we cannot compare the absolute performance of a FSOD method on Pascal VOC and DOTA and the latter extrapolation is not valid.

Nevertheless, there is a pattern: FSOD methods work consistently better on natural images compared to aerial images. To understand this phenomenon, we need a way to fairly compare the FSOD performance across several datasets. To this end, we propose to look at the relative performance of the FSOD methods against the non few-shot baseline (i.e. FCOS in our case) using the following metric:

$$RmAP = \frac{mAP_{FSOD} - mAP_{Baseline}}{mAP_{Baseline}}. \quad (6)$$

This metric assesses how well a FSOD method is performing on different datasets even if the classical detection performance differs. Hence, it represents how much performance is lost when switching from regular to the few-shot regime. This is exactly what is illustrated in Fig. 3, white percentages are RmAP values. RmAP is significantly lower on DOTA and DIOR compared to Pascal VOC. This way, we can quantitatively confirm the intuition emerging from the above results: FSOD works better on natural images.

We hypothesize that this performance gap is mainly due to differences in the objects sizes within the datasets. In aerial images, objects are much smaller in average. While this is already an issue for object detection, the problem is amplified for FSOD as it is difficult to extract semantic information from small objects in support examples. To support our hypothesis, we first conduct a brief size analysis of the three datasets DOTA, DIOR, Pascal VOC and MS COCO (see Fig. 4). Aerial datasets contain far smaller objects than natural ones. Plus, in aerial datasets the size of objects in different classes differs a lot. Some classes contain only small objects, while others only large objects. In Pascal VOC, this class’ size variance is limited. We argue that it is more difficult for the model to extract relevant information from small support examples but also to learn more diverse features to deal with a greater objects’ size variance. This partly explains the greater difficulty of MS COCO.

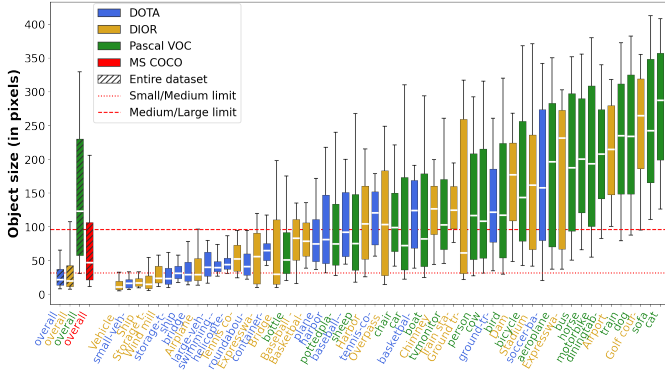


Fig. 4. Box plot of objects size in DOTA, DIOR and Pascal VOC and MS COCO. On the left side, boxes represent the overall size distribution in each dataset. On the right side, the distributions are split by class and ordered by average size. As MS COCO contains 80 classes, we chose not to include the per class box plots for it in this plot.

To support this claim, we conduct a per-class performance analysis on DOTA, DIOR and Pascal VOC. The results of this comparison are available in Fig. 5. In this figure, the performance is reported per class against the average size of the class. The first row reports absolute mAP values both for FRW and FCOS (baseline). In the second, the mAP gap between the FRW and the baseline is plotted against the objects’ size. We did not report RmAP values for the sake of visualization. RmAP can take large value (e.g. when baseline mAP is low) and this squeezes the interesting part of the plot in a narrow band around 0. The same plot with RmAP is available in Appendix F. Larger objects are easier to detect, even without few-shot. This trend is accentuated in the few-shot regime (in the first row, the blue trend lines are steeper than the blacks). This is observed for base classes but not always for novel classes, probably because the trends on novel classes are not reliable due to the limited number of points. Fig. 12 in Appendix F shows a more reliable trend for novel classes when the results from the three datasets are aggregated. Finally, the few-shot inference, which leverage support information to condition the detection can surpass the baseline in some cases. For base classes, the model benefits from having examples available at test time only when the objects are large. On the contrary, when the objects are small, this inference mode is detrimental. For novel classes, however, the performance is always below the baseline, even if the gap shrinks with larger objects. This is expected as the network only received a weak supervision for these classes.

This comparative analysis confirms that detecting small objects is a very difficult task in the few-shot regime. It is hard to extract useful information from small support objects. Even worse, this information can be detrimental for the detection. Existing FSOD methods are not designed to deal with small objects, hence the application of these methods on aerial images does not yield satisfactory results. It is therefore crucial to develop FSOD techniques that target specifically small objects. We propose a first attempt in this direction in Sec. 5.

5 CROSS-SCALES QUERY-SUPPORT ALIGNMENT FOR SMALL FSOD

From the analysis in Sec. 4.2, it is clear that a new attention mechanism specifically designed for small objects is required to get reasonable performance on aerial images. To this end, we propose a novel alignment method that combines information from multiple scales: Cross-Scales Query-Support Alignment (XQSA). This differs from existing methods which often work independently at different scales. First, all query features (i.e. from different levels) are flattened and concatenated. Then, they are linearly projected into the queries, keys and values matrices Q , K and V :

$$\begin{aligned}
 \text{Concatenated} & \downarrow \\
 \text{multiscale features} & \downarrow \\
 Q &= F_q W_Q = [F_{q,0}, F_{q,1}, F_{q,2}] W_Q, & (7) \\
 K^c &= F_s^c W_K = [F_{s,0}^c, F_{s,1}^c, F_{s,2}^c] W_K, & (8) \\
 V^c &= F_s^c W_V = [F_{s,0}^c, F_{s,1}^c, F_{s,2}^c] W_V. & (9)
 \end{aligned}$$

↑
 Learned projection matrices

From this, an affinity matrix is computed between the queries and the keys, and then the aligned support features are computed as:

$$\lambda^c = \text{Softmax}\left(\frac{QK^{cT}}{\sqrt{d}}\right), \quad (10)$$

$$A_q^c = \lambda^c V^c. \quad (11)$$

The aligned features are finally processed by a two-layers MLP with skip connections. LayerNorm [63] is applied before alignment and the MLP. It can be seen as a learnable fusion operation in the AAF framework, similar to what was proposed in [7], [34], [43] (see Tab. 1). This resembles the ViT attention, but with a major difference, it combines features from different images and different levels (see Fig. 6). This allows to better match objects of different sizes in the support and the query images.

Small objects have a limited footprint in feature maps which make them hard to detect but also hard to match with support examples. XQSA’s multiscale alignment enhances the chances of matching as each query feature is compared with support features at all scales. Finally, in order to fairly compare with DANA, we leverage their Background Attenuation block (BGA) on the support features before alignment. They conduct a thorough ablation study which shows the positive impact of BGA on the few-shot performance of their method. We also carry out an ablation study about our cross-scales method (see Appendix H) and find that BGA also improves performance in this case. XQSA is implemented inside the AAF framework, split into three modules: alignment, attention and fusion, following the description from Sec. 3.

To assess the capabilities of the proposed method, we compare it with the best methods from Sec. 4.2: FRW and DANA on DOTA, DIOR and Pascal VOC (see Appendix G for results with $\text{mAP}_{0.5:0.95}$ and on MS COCO). The results of these experiments are available in Tab. 5. The mAP values are reported separately for small ($\sqrt{wh} < 32$),

TABLE 5

Comparison of the performance between the proposed XQSA alignment method and the two best reimplemented methods on DOTA and DIOR, FRW and DANA. mAP_{0.5} values are reported separately for base and novel classes on DOTA, DIOR and Pascal VOC. Results with mAP_{0.5} and on MS COCO are also available in Appendix G. As XQSA is specifically designed for small objects, mAP values are reported for All, Small ($\sqrt{wh} < 32$), Medium ($32 \leq \sqrt{wh} < 96$) and Large ($\sqrt{wh} \geq 96$) objects. All experiments were conducted with $K = 10$ shots.

	DOTA								DIOR								Pascal VOC							
	Base				Novel				Base				Novel				Base				Novel			
	All	S	M	L	All	S	M	L	All	S	M	L	All	S	M	L	All	S	M	L	All	S	M	L
FRW	0.49	0.25	0.59	0.63	0.37	0.14	0.34	0.59	0.62	0.08	0.49	0.81	0.36	0.02	0.34	0.59	0.63	0.16	0.48	0.82	0.49	0.16	0.27	0.68
DANA	0.54	0.37	0.62	0.70	0.36	0.14	0.40	0.65	0.63	0.11	0.49	0.83	0.38	0.03	0.35	0.61	0.65	0.18	0.51	0.80	0.52	0.10	0.25	0.67
XQSA	0.51	0.26	0.59	0.64	0.41	0.18	0.45	0.54	0.60	0.11	0.46	0.82	0.42	0.04	0.41	0.58	0.62	0.16	0.49	0.76	0.54	0.19	0.35	0.66

medium ($32 \leq \sqrt{wh} < 96$) and large ($\sqrt{wh} \geq 96$) objects. Hence, the methods can be compared specifically on small objects. XQSA performs consistently better on small and medium novel objects, compared with FRW and DANA. This is mitigated on base classes, but it is not surprising, the large number of available examples is enough to learn a robust query-support matching even for small objects. In some cases, it is worse than the other methods for base classes. While allowing matching across different scales, XQSA also brings more mismatches. For base classes, with strong supervision, the benefits of the multiscale matching may not compensate the drawbacks associated. On large objects, the performance is a bit lower with XQSA. Probably for the same reasons as for base classes, large objects are already well handled by existing FSOD techniques and in this case the multiscale matching is not worth it. Looking at the performance on all objects, the proposed alignment technique improves significantly the detection quality for aerial images. Using XQSA in the AAF framework increased novel class mAP by 0.05 on DOTA and 0.04 on DIOR. As it works better on small objects but worse on large objects, it is less appropriate for natural images. As a consequence, it shows lower improvements for Pascal VOC and MS COCO.

Overall, the proposed method largely improves on existing works for aerial images. On DIOR, this corresponds to a 0.1 mAP increase compared to previous state-of-the-art [4]. However, this is not sufficient to fill the performance gap with natural images as presented in Appendix F. While XQSA improves on other methods on aerial images, it is still far behind the performance of the baseline without few-shot. XQSA is better for small objects but at the cost of lower performance on large objects and base classes. Progresses are still required to get more versatile FSOD solutions able to handle small, medium, and large objects.

6 CONCLUSION AND FUTURE WORK

In a nutshell, our review of attention-based FSOD emphasizes the variety of methods in the literature and the lack of application on aerial images. Comparison between FSOD methods is difficult as many details change from a method to another. This makes it impractical to find the most suitable method for a given problem or dataset. Our proposed framework solves this issue by providing a fixed but modular environment to benchmark attention-based FSOD methods. Using this framework, we conduct several comparisons on various datasets. We also provide a novel metric, Relative mAP (RmAP), specifically designed to assess how good a FSOD method is compared with its non few-shot counterpart. This metric allows comparison

between different datasets, which highlights different behaviors for FSOD methods on natural and aerial images. Our experiments provide evidences toward the nature of these discrepancies. Small objects are notoriously difficult to detect, but in the few-shot regime they are even more challenging as the query-support matching is harder for them. To close the performance gap between small, medium and large objects, we propose a novel multiscale alignment method named XQSA. It is designed to enlarge the matching possibilities across different feature levels. This improves significantly the performance on small and medium objects, yielding large improvements over the state-of-the-art on DOTA and DIOR datasets. However, this comes at the expense of lower performance on large objects and base classes. Future works should thus focus on developing more versatile FSOD techniques able to deal both with small and large objects. This work shed some light on the challenging small few-shot object detection problem and provide tools for deeper analysis and the development of more universal attention based FSOD methods.

ACKNOWLEDGMENTS

The authors would like to thank COSE company for their close collaboration and the funding of this project.

REFERENCES

- [1] S. Ren, K. He, R. Girshick, and J. Sun, "Faster r-cnn: Towards real-time object detection with region proposal networks," *Advances in neural information processing systems*, vol. 28, pp. 91–99, 2015.
- [2] J. Redmon, S. Divvala, R. Girshick, and A. Farhadi, "You only look once: Unified, real-time object detection," in *Proceedings of the IEEE conference on computer vision and pattern recognition*, 2016, pp. 779–788.
- [3] B. Kang, Z. Liu, X. Wang, F. Yu, J. Feng, and T. Darrell, "Few-shot object detection via feature reweighting," in *Proceedings of the IEEE/CVF International Conference on Computer Vision*, 2019, pp. 8420–8429.
- [4] X. Li, J. Deng, and Y. Fang, "Few-shot object detection on remote sensing images," *IEEE Transactions on Geoscience and Remote Sensing*, pp. 1–14, 2021.
- [5] Q. Fan, W. Zhuo, C.-K. Tang, and Y.-W. Tai, "Few-shot object detection with attention-rpn and multi-relation detector," in *Proceedings of the IEEE/CVF Conference on Computer Vision and Pattern Recognition*, 2020, pp. 4013–4022.
- [6] T.-I. Hsieh, Y.-C. Lo, H.-T. Chen, and T.-L. Liu, "One-shot object detection with co-attention and co-excitation," in *Advances in Neural Information Processing Systems 32*, 2019.
- [7] X. Li, L. Zhang, Y. P. Chen, Y.-W. Tai, and C.-K. Tang, "One-shot object detection without fine-tuning," *arXiv preprint arXiv:2005.03819*, 2020.
- [8] M. Everingham, L. Van Gool, C. K. Williams, J. Winn, and A. Zisserman, "The pascal visual object classes (voc) challenge," *International journal of computer vision*, vol. 88, no. 2, pp. 303–338, 2010.

- [9] T.-Y. Lin, M. Maire, S. Belongie, J. Hays, P. Perona, D. Ramanan, P. Dollár, and C. L. Zitnick, "Microsoft coco: Common objects in context," in *European conference on computer vision*. Springer, 2014, pp. 740–755.
- [10] G.-S. Xia, X. Bai, J. Ding, Z. Zhu, S. Belongie, J. Luo, M. Datcu, M. Pelillo, and L. Zhang, "Dota: A large-scale dataset for object detection in aerial images," in *Proceedings of the IEEE Conference on Computer Vision and Pattern Recognition*, 2018, pp. 3974–3983.
- [11] K. Li, G. Wan, G. Cheng, L. Meng, and J. Han, "Object detection in optical remote sensing images: A survey and a new benchmark," *ISPRS Journal of Photogrammetry and Remote Sensing*, vol. 159, pp. 296–307, 2020.
- [12] T.-Y. Lin, P. Goyal, R. Girshick, K. He, and P. Dollár, "Focal loss for dense object detection," in *Proceedings of the IEEE international conference on computer vision*, 2017, pp. 2980–2988.
- [13] Z. Tian, C. Shen, H. Chen, and T. He, "Fcos: Fully convolutional one-stage object detection," in *Proceedings of the IEEE/CVF International Conference on Computer Vision*, 2019, pp. 9627–9636.
- [14] T.-Y. Lin, P. Dollár, R. Girshick, K. He, B. Hariharan, and S. Belongie, "Feature pyramid networks for object detection," in *Proceedings of the IEEE conference on computer vision and pattern recognition*, 2017, pp. 2117–2125.
- [15] X. Dai, Y. Chen, B. Xiao, D. Chen, M. Liu, L. Yuan, and L. Zhang, "Dynamic head: Unifying object detection heads with attentions," in *Proceedings of the IEEE/CVF Conference on Computer Vision and Pattern Recognition*, 2021, pp. 7373–7382.
- [16] N. Carion, F. Massa, G. Synnaeve, N. Usunier, A. Kirillov, and S. Zagoruyko, "End-to-end object detection with transformers," in *European Conference on Computer Vision*. Springer, 2020, pp. 213–229.
- [17] Y. Wang, Q. Yao, J. T. Kwok, and L. M. Ni, "Generalizing from a few examples: A survey on few-shot learning," *ACM Computing Surveys (CSUR)*, vol. 53, no. 3, pp. 1–34, 2020.
- [18] J. Kirkpatrick, R. Pascanu, N. Rabinowitz, J. Veness, G. Desjardins, A. A. Rusu, K. Milan, J. Quan, T. Ramalho, A. Grabska-Barwinska et al., "Overcoming catastrophic forgetting in neural networks," *Proceedings of the national academy of sciences*, vol. 114, no. 13, pp. 3521–3526, 2017.
- [19] C. Finn, P. Abbeel, and S. Levine, "Model-agnostic meta-learning for fast adaptation of deep networks," in *International Conference on Machine Learning*. PMLR, 2017, pp. 1126–1135.
- [20] S. R. H. Larochelle, "Optimization as a model for few-shot learning," in *5th International Conference on Learning Representations, ICLR 2017, Toulon, France, April 24–26, 2017, Conference Track Proceedings*, 2017.
- [21] J. Snell, K. Swersky, and R. Zemel, "Prototypical networks for few-shot learning," in *Advances in Neural Information Processing Systems*, I. Guyon, U. V. Luxburg, S. Bengio, H. Wallach, R. Fergus, S. Vishwanathan, and R. Garnett, Eds., vol. 30, 2017.
- [22] L. Bertinetto, J. F. Henriques, J. Valmadre, P. Torr, and A. Vedaldi, "Learning feed-forward one-shot learners," in *Advances in neural information processing systems*, 2016, pp. 523–531.
- [23] J. Hu, L. Shen, and G. Sun, "Squeeze-and-excitation networks," in *Proceedings of the IEEE conference on computer vision and pattern recognition*, 2018, pp. 7132–7141.
- [24] X. Wang, R. Girshick, A. Gupta, and K. He, "Non-local neural networks," in *Proceedings of the IEEE conference on computer vision and pattern recognition*, 2018, pp. 7794–7803.
- [25] A. Dosovitskiy, L. Beyer, A. Kolesnikov, D. Weissenborn, X. Zhai, T. Unterthiner, M. Dehghani, M. Minderer, G. Heigold, S. Gelly, J. Uszkoreit, and N. Houlsby, "An image is worth 16x16 words: Transformers for image recognition at scale," in *International Conference on Learning Representations*, 2021. [Online]. Available: <https://openreview.net/forum?id=YicbFdNTTy>
- [26] C. Doersch, A. Gupta, and A. Zisserman, "Crosstransformers: spatially-aware few-shot transfer," *arXiv preprint arXiv:2007.11498*, 2020.
- [27] X. Yan, Z. Chen, A. Xu, X. Wang, X. Liang, and L. Lin, "Meta r-cnn: Towards general solver for instance-level low-shot learning," in *Proceedings of the IEEE/CVF International Conference on Computer Vision*, 2019, pp. 9577–9586.
- [28] Q. Fan, W. Zhuo, C.-K. Tang, and Y.-W. Tai, "Few-shot object detection with attention-rpn and multi-relation detector," in *CVPR*, 2020.
- [29] Y. Xiao and R. Marlet, "Few-shot object detection and viewpoint estimation for objects in the wild," in *European Conference on Computer Vision*. Springer, 2020, pp. 192–210.
- [30] Z. Xiao, J. Qi, W. Xue, and P. Zhong, "Few-shot object detection with self-adaptive attention network for remote sensing images," *IEEE Journal of Selected Topics in Applied Earth Observations and Remote Sensing*, vol. 14, pp. 4854–4865, 2021.
- [31] G. Kim, H.-G. Jung, and S.-W. Lee, "Few-shot object detection via knowledge transfer," in *2020 IEEE International Conference on Systems, Man, and Cybernetics (SMC)*, 2020, pp. 3564–3569.
- [32] D. A. Ganea, B. Boom, and R. Poppe, "Incremental few-shot instance segmentation," in *Proceedings of the IEEE/CVF Conference on Computer Vision and Pattern Recognition*, 2021, pp. 1185–1194.
- [33] Y. Gao, R. Hou, Q. Gao, and Y. Hou, "A fast and accurate few-shot detector for objects with fewer pixels in drone image," *Electronics*, vol. 10, no. 7, p. 783, 2021.
- [34] G. Han, S. Huang, J. Ma, Y. He, and S.-F. Chang, "Meta faster r-cnn: Towards accurate few-shot object detection with attentive feature alignment," *arXiv preprint arXiv:2104.07719*, 2021.
- [35] G. Zhang, Z. Luo, K. Cui, and S. Lu, "Meta-detr: Few-shot object detection via unified image-level meta-learning," *arXiv preprint arXiv:2103.11731*, 2021.
- [36] W. Liu, H. Li, S. Yu, S. Chen, X. Ye, J. Wu et al., "Dynamic relevance learning for few-shot object detection," *arXiv preprint arXiv:2108.02235*, 2021.
- [37] T.-I. Chen, Y.-C. Liu, H.-T. Su, Y.-C. Chang, Y.-H. Lin, J.-F. Yeh, and W. H. Hsu, "Should i look at the head or the tail? dual-awareness attention for few-shot object detection," *arXiv preprint arXiv:2102.12152*, 2021.
- [38] H. Xu, X. Wang, F. Shao, B. Duan, and P. Zhang, "Few-shot object detection via sample processing," *IEEE Access*, vol. 9, pp. 29 207–29 221, 2021.
- [39] J. Chu, J. Feng, P. Jing, and W. Lu, "Joint co-attention and co-reconstruction representation learning for one-shot object detection," in *2021 IEEE International Conference on Image Processing (ICIP)*, 2021, pp. 2229–2233.
- [40] A. Li and Z. Li, "Transformation invariant few-shot object detection," in *Proceedings of the IEEE/CVF Conference on Computer Vision and Pattern Recognition*, 2021, pp. 3094–3102.
- [41] G. Han, J. Ma, S. Huang, L. Chen, and S.-F. Chang, "Few-shot object detection with fully cross-transformer," in *Proceedings of the IEEE/CVF Conference on Computer Vision and Pattern Recognition*, 2022, pp. 5321–5330.
- [42] G. Zhang, K. Cui, R. Wu, S. Lu, and Y. Tian, "Pnpdet: Efficient few-shot detection without forgetting via plug-and-play sub-networks," in *Proceedings of the IEEE/CVF Winter Conference on Applications of Computer Vision*, 2021, pp. 3823–3832.
- [43] A. Wu, Y. Han, L. Zhu, and Y. Yang, "Universal-prototype enhancing for few-shot object detection," in *Proceedings of the IEEE/CVF International Conference on Computer Vision*, 2021, pp. 9567–9576.
- [44] L. Liu, B. Wang, Z. Kuang, J.-H. Xue, Y. Chen, W. Yang, Q. Liao, and W. Zhang, "Gendet: Meta learning to generate detectors from few shots," *IEEE Transactions on Neural Networks and Learning Systems*, 2021.
- [45] L. Karlinsky, J. Shtok, S. Harary, E. Schwartz, A. Aides, R. Feris, R. Giryes, and A. M. Bronstein, "Repmet: Representative-based metric learning for classification and few-shot object detection," in *Proceedings of the IEEE/CVF Conference on Computer Vision and Pattern Recognition*, 2019, pp. 5197–5206.
- [46] Y. Yang, F. Wei, M. Shi, and G. Li, "Restoring negative information in few-shot object detection," *Advances in neural information processing systems*, vol. 33, pp. 3521–3532, 2020.
- [47] B. Sun, B. Li, S. Cai, Y. Yuan, and C. Zhang, "Fsce: Few-shot object detection via contrastive proposal encoding," in *Proceedings of the IEEE/CVF Conference on Computer Vision and Pattern Recognition*, 2021, pp. 7352–7362.
- [48] P. L. Jeune, M. Lebbah, A. Mokraoui, and H. Azzag, "Experience feedback using representation learning for few-shot object detection on aerial images," in *2021 20th IEEE International Conference on Machine Learning and Applications (ICMLA)*, 2021, pp. 662–667.
- [49] Y. Cao, J. Wang, Y. Jin, T. Wu, K. Chen, Z. Liu, and D. Lin, "Few-shot object detection via association and discrimination," *Advances in Neural Information Processing Systems*, vol. 34, pp. 16 570–16 581, 2021.
- [50] A. Wu, S. Zhao, C. Deng, and W. Liu, "Generalized and discriminative few-shot object detection via svd-dictionary enhancement," *Advances in Neural Information Processing Systems*, vol. 34, pp. 6353–6364, 2021.

- [51] H. Chen, Y. Wang, G. Wang, and Y. Qiao, "Lstd: A low-shot transfer detector for object detection," in *Proceedings of the AAAI Conference on Artificial Intelligence*, vol. 32, no. 1, 2018.
- [52] Z. Fan, Y. Ma, Z. Li, and J. Sun, "Generalized few-shot object detection without forgetting," in *Proceedings of the IEEE/CVF Conference on Computer Vision and Pattern Recognition*, 2021, pp. 4527–4536.
- [53] X. Wang, T. E. Huang, T. Darrell, J. E. Gonzalez, and F. Yu, "Frustratingly simple few-shot object detection," in *International Conference on Machine Learning (ICML)*, July 2020.
- [54] J. Wu, S. Liu, D. Huang, and Y. Wang, "Multi-scale positive sample refinement for few-shot object detection," in *European Conference on Computer Vision*. Springer, 2020, pp. 456–472.
- [55] A. Bar, X. Wang, V. Kantorov, C. J. Reed, R. Herzig, G. Chechik, A. Rohrbach, T. Darrell, and A. Globerson, "Detreg: Unsupervised pretraining with region priors for object detection," in *Proceedings of the IEEE/CVF Conference on Computer Vision and Pattern Recognition*, 2022, pp. 14605–14615.
- [56] W. Zhang and Y.-X. Wang, "Hallucination improves few-shot object detection," in *Proceedings of the IEEE/CVF Conference on Computer Vision and Pattern Recognition*, 2021, pp. 13008–13017.
- [57] S. Wolf, J. Meier, L. Sommer, and J. Beyerer, "Double head predictor based few-shot object detection for aerial imagery," in *Proceedings of the IEEE/CVF International Conference on Computer Vision*, 2021, pp. 721–731.
- [58] X. Huang, B. He, M. Tong, D. Wang, and C. He, "Few-shot object detection on remote sensing images via shared attention module and balanced fine-tuning strategy," *Remote Sensing*, vol. 13, no. 19, p. 3816, 2021.
- [59] Y. Xu, B. Huang, X. Luo, K. Bradbury, and J. M. Malof, "Simpl: Generating synthetic overhead imagery to address zero-shot and few-shot detection problems," 2021. [Online]. Available: <https://arxiv.org/abs/2106.15681>
- [60] A. Vaswani, N. Shazeer, N. Parmar, J. Uszkoreit, L. Jones, A. N. Gomez, Ł. Kaiser, and I. Polosukhin, "Attention is all you need," in *Advances in neural information processing systems*, 2017, pp. 5998–6008.
- [61] G. Huang, I. Laradji, D. Vazquez, S. Lacoste-Julien, and P. Rodriguez, "A survey of self-supervised and few-shot object detection," *arXiv preprint arXiv:2110.14711*, 2021.
- [62] A. M. Pierre Le Jeune, "Improving few-shot object detection through a performance analysis on aerial and natural images," in *Proceedings of the 30th European Signal Processing Conference (EUSIPCO)*, 2022.
- [63] J. L. Ba, J. R. Kiros, and G. E. Hinton, "Layer normalization," *arXiv preprint arXiv:1607.06450*, 2016.



Anissa MOKRAOUI received the state engineering degree in electrical engineering from national school of telecommunications in 1989 from Algeria, the M.S degree in information technology in 1990 and the Ph.D. degree in 1994 both from University Paris 11, Orsay France. From 92 to 94, she worked at the National Institute of Telecommunications (INT, at Evry France) where her research activities were on digital signal processing, fast filtering algorithms and implementation problems on DSP. In 1997, she was appointed as assistant professor and in December 2011 as associate professor at Galilé Institute of University Paris 13, France. Since 2013, she is full professor at Galilé Institute of Université Sorbonne Paris Nord (USPN), France. Since 2016, she is the director of the L2TI laboratory of USPN. Her current research interests include source coding (image, video, multi-view, stereoscopic); joint source-channel-protocol decoding, robust mobile transmission, MIMO-OFDM channel estimation (massive), computer vision, few-shot object detection. She is co-author of more than 150 contributions to journals and conference proceedings. She served on program committees for conferences. She acts as a reviewer for many IEEE and EURASIP conferences and journals.



Pierre LE JEUNE is a PhD student at L2TI laboratory, University Sorbonne Paris Nord while working at COSE company. He received the M.Sc. degree in Mathematical Modelling and Computation from Danish Technical University and the M.Sc. in Engineering from Centrale Nantes. His current research interests include Few-Shot Learning, Computer Vision and Deep Learning.

APPENDIX A NOVEL CLASSES SPLITS

The base/novel classes split is crucial to compare the performance reported for FSOD methods. This appendix reports the splits used in our experiments. The human-readable labels are not included in the following table to keep the size constrained, but they can be found on datasets’ project pages.

TABLE 6
Base / Novel class splits for the different datasets used in this work.

	Novel classes	Base classes
Pascal VOC	3,6,10,14,18 1,2,3,4,5, 6,7,9,15,16,	1,2,4,5,7,8,9,11,12,13,15,16,17,19,20 8,10,11,12,13,14,21,22,23,24, 25,26,27,28,29,30,31,32,33,34,
MS COCO	17,18,19,20,40, 57,58,59,61,63	35,36,37,38,39,41,42,43,44,45, 46,47,48,49,50,51,52,53,54,55, 56,60,62,64,65,66,67,68,69,70, 71,72,73,74,75,76,77,78,79,80
DOTA	3,5,15	1,2,4,6,7,8,9,10,11,12,13,14,16
DIOR	1,3,17,18,20	2,4,5,6,7,8,9,10,11,12,13,14,15,16,19

APPENDIX B OBJECT-LEVEL AUGMENTATIONS

To improve the performance of the methods implemented in the AAF framework and be competitive with existing works, we propose an augmentation pipeline specifically designed for detection. Some regular augmentation techniques cannot be directly applied for object detection as it can completely mask objects from the image. This deteriorates the training as the model will not be able to detect hidden objects, but it will be penalized anyway.

First, we apply random horizontal and vertical flips (only for aerial images) and color jitter. As it does not remove entire objects, these can be applied directly on the images. Unlike some other classical techniques such as random crop-resize and random cut-out cannot. Therefore, we developed object-preserving random crop-resize and cut-out. The main idea is to apply these transformations at the object level and not at the image level. This ensures that objects of interest are still visible in the transformed image. For crop-resize, a non-empty subset of the objects in the image is randomly sampled. An overall bounding box is computed around all these objects and the cropped area is randomly drawn between this box and the image borders. Hence, it guarantees the presence of at least one object inside the cropped image. For cut-out, the principle is similar, instead of cutting out a random part of the image, the cut is applied at the object level so that it does not hide out entire objects. Fig. 7 compares the two proposed augmentations with their naive implementations.

We performed a cumulative study to assess the benefits of each component of the augmentation pipeline. This is summarized in Tab. 7. It shows that the augmentation is beneficial for the performance on novel classes but detrimental for base classes with augmentation. More specifically,

it seems that image flips are responsible for the performance loss on base classes (see first and second columns in Tab. 7). Base classes performance drops when adding flips but remains mostly constant when adding other types of augmentations. One crucial difference between flip and other augmentations is that we chose to apply flips also on support examples. This choice was made to increase the diversity of the support set during fine-tuning. For novel classes, only a few images are available as support during fine-tuning, and we want to avoid overfitting these examples. Although other types of augmentation could have been employed for this as well, we wanted to prevent disrupting too much the information in the support. This choice may be the cause of the performance drop on base classes. To verify this hypothesis, we conduct a few more experiments disabling the flip in the support set. With the *default* cropping strategy, the experiments confirm the hypothesis: no performance drop is observed when supports are not flipped. However, as this certainly interacts with the cropping strategy, we also tried with *same-size* as it is the chosen strategy for most experiments in this paper (see Appendix C). Surprisingly, it does not produce similar results, and in this case, flips in supports are actually beneficial for base classes performance. This suggests a complex interaction between augmentation on the support set and the cropping strategy. The choice made in this paper may not be optimal in this regard, and a deeper analysis of this interaction should be conducted as future work. Finally, the base class performance loss is compensated by clear improvements on novel classes. As this is the main goal of FSOD, we chose to adopt the original augmentation pipeline, i.e. with flips in support, for our experiments.

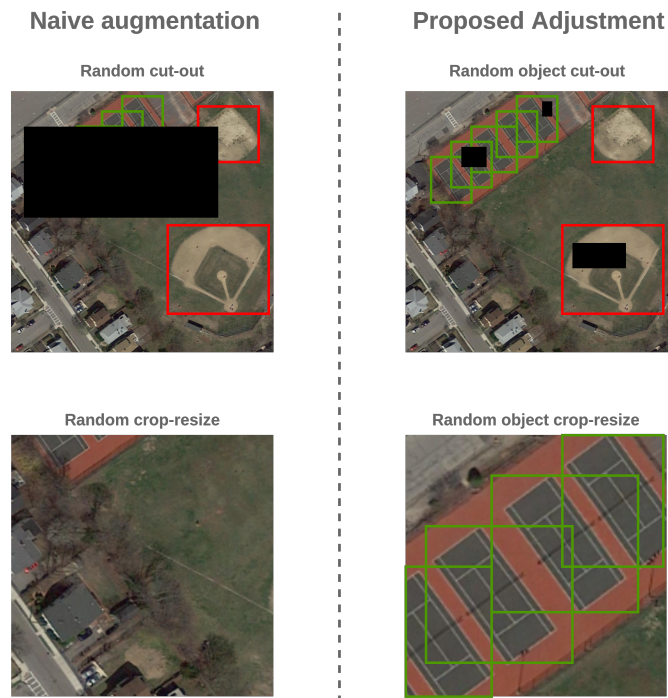


Fig. 7. Difference between naive augmentation techniques (left) and our adaptation to object detection (right). The proposed transformations are applied at the object-level to preserve objects integrity.

TABLE 7

Cumulative study of the proposed augmentation techniques on DOTA with FRW method. $\text{mAP}_{0.5}$ is reported for different number of shots.

# Shots		Baseline	+ Flip	+ Color	+ Cutout	+ Crop
1	Base	0.488	0.458	0.460	0.472	0.457
	Novel	0.062	0.052	0.069	0.064	0.100
3	Base	0.511	0.475	0.470	0.461	0.452
	Novel	0.144	0.186	0.186	0.197	0.220
5	Base	0.527	0.494	0.501	0.503	0.487
	Novel	0.193	0.237	0.251	0.250	0.259
10	Base	0.538	0.508	0.508	0.504	0.503
	Novel	0.286	0.312	0.281	0.341	0.359

APPENDIX C

SUPPORT EXTRACTION STRATEGIES

The support information is located only inside a delimited area of the support image, its corresponding bounding box. The remaining part of the image mostly contains irrelevant information concerning the object class. Therefore, extracting features from the whole support images is not necessary. But features contained only inside the object’s bounding box might not be sufficient as well. Context can be extremely valuable in certain cases, especially for small objects. For instance, a car and a small boat could easily be mistaken without context. Close surroundings of the objects can help for recognition.

The most common strategy for support information extraction is proposed by [3]. They concatenate the whole support image with the support object’s binary mask (rectangular, computed from the bounding box) and pass this to an extractor network. This has two main drawbacks. First, it is necessary to compute feature from the entire support image, which is a loss of resources. Second, the same network cannot be used for extracting features in query and support images as it needs an additional input channel to process the mask. Hence, the network cannot be pretrained beforehand. This design choice is rarely discussed, if ever mentioned, in the literature.

In this appendix, we explore this design choice by implementing several extraction strategies. We did not reimplement the technique from [3] as it requires to have two different networks for support and query feature extraction. However, some of our techniques are quite close from what they proposed. These techniques are described bellow and Fig. 9 illustrates most of them.

- **Default:** the most naive extraction technique. It consists in cropping the support image around the support object at a fixed size (e.g. 128×128). Objects larger than this are simply resized to fit in the patch.
- **Context-padding:** the cropping occurs exactly as with the default strategy, but areas around the objects are masked out. This is close to what was proposed by [3].
- **Reflection:** context is replaced by reflection of the object. In the case of small objects, the support patch can easily be dominated either by irrelevant information or by zeros when using the latter two extraction methods.
- **Same-size:** all objects are resized to fill entirely the support patch (preserving the aspect ratio). It does not change the process for large objects, but it prevents smaller objects to be dominated by irrelevant information.

- **Multi-scale:** the object is resized and cropped at 3 different scales. Each scale is responsible for matching small, medium and large objects in query images.
- **Mixed:** it is a combination of the default strategy and *same-size*. Small objects (i.e. $\sqrt{wh} < 32$) are extracted using the default strategy. Larger objects ($\sqrt{wh} \geq 32$) are resized into a patch of 128×128 pixels. Hence, small objects are not upsampled more than 4 times, as they are using the *resize* strategy.

These strategies are compared in Table 8. Even though *same-size* gets the best overall results on novel classes (regardless of object sizes), there is no clear conclusion. It is outperformed by both *reflection* and *mixed* for base classes. No method outperforms the others on all object sizes, not even the ones designed to be more robust to size (*multiscale* and *mixed*). The latter two techniques introduce discrepancies in the features: objects of similar sizes can be processed differently and give different features. It is probably easier for the network to learn semantic representations from objects of the same size. As *same-size* gives the best results on novel classes, we chose to use this one for all our experiments.

However, in the light of our performance analysis in Sec. 4.2, we can understand some results from Tab. 8. The *multiscale* strategy does not perform very well as it introduces small objects features which seem detrimental for the good conditioning of the network. On the contrary, *same-size* only generates large objects as support which is a better strategy. Finally, *reflection* performs surprisingly well for small objects while preserving their small size. The redundancy generated by the reflection of such small objects reinforces the object’s features.

TABLE 8

Comparison of support extraction strategies on base and novel classes with DOTA dataset and FRW method with 10 shots. $\text{mAP}_{0.5}$ is reported on all objects and separately on objects of different sizes: small (S), medium (M) and large (L).

	Base classes				Novel classes			
	All	S	M	L	Mean	S	M	L
Default	0.498	0.243	0.574	0.639	0.250	0.077	0.243	0.345
Context padding	0.500	0.250	0.597	0.630	0.296	0.107	0.268	0.509
Same-size	0.506	0.308	0.594	0.625	0.322	0.083	0.332	0.565
Multiscale	0.514	0.290	0.598	0.633	0.270	0.084	0.335	0.456
Reflection	0.503	0.261	0.594	0.625	0.255	0.072	0.207	0.443
Mixed	0.509	0.272	0.605	0.607	0.280	0.095	0.265	0.489

APPENDIX D

RESULTS FROM ORIGINAL PAPERS ON PASCAL VOC AND MS COCO

In this appendix, we report the results on Pascal VOC and MS COCO of the different methods to be compared with our results achieved in our framework: FRW [3], WSAAN [30], DANA [37], MFRCN [34] and DRL [36]. These results can be found in Tab. 9 and Tab. 10. This demonstrates the lack of comparative study in the literature, most methods are designed and evaluated with different datasets and metrics. In addition, we indicate in the table the backbone used by each method to highlights the differences preventing a good comparison. However, plenty of other details change as well. As an example, DRL leverages a dynamic relation matrix between support and query features, solely for the computation of an auxiliary loss function.

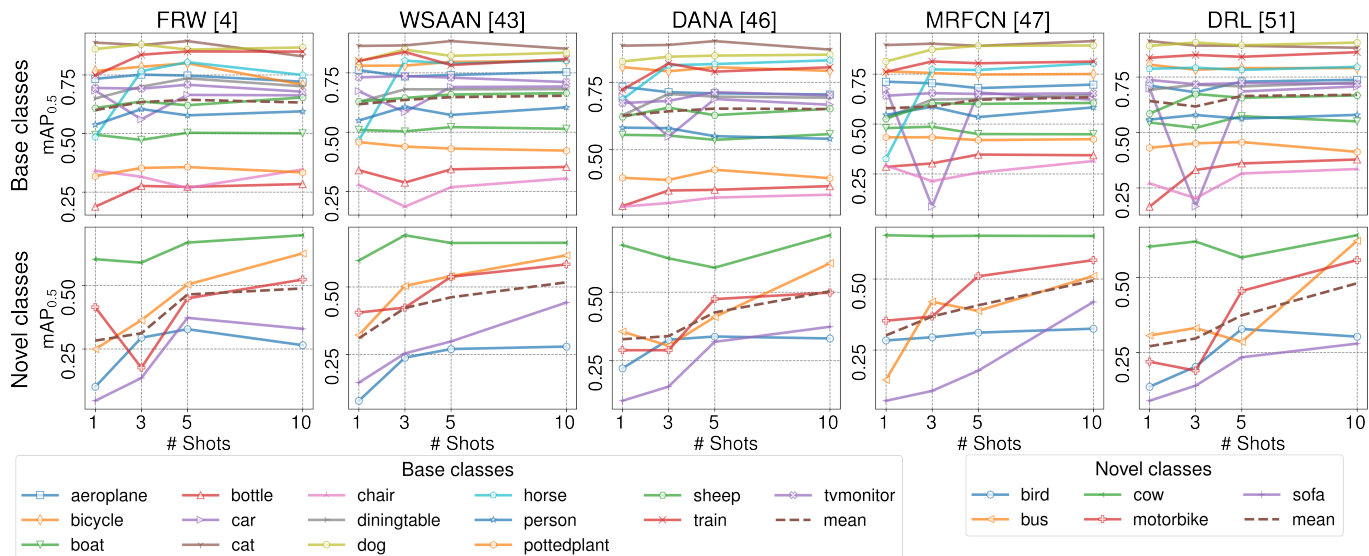


Fig. 8. $mAP_{0.5}$ on Pascal VOC against the number of shots for each class and each method. Dashed lines represent average performance on all classes, either base classes (**top**) or novel classes (**bottom**).

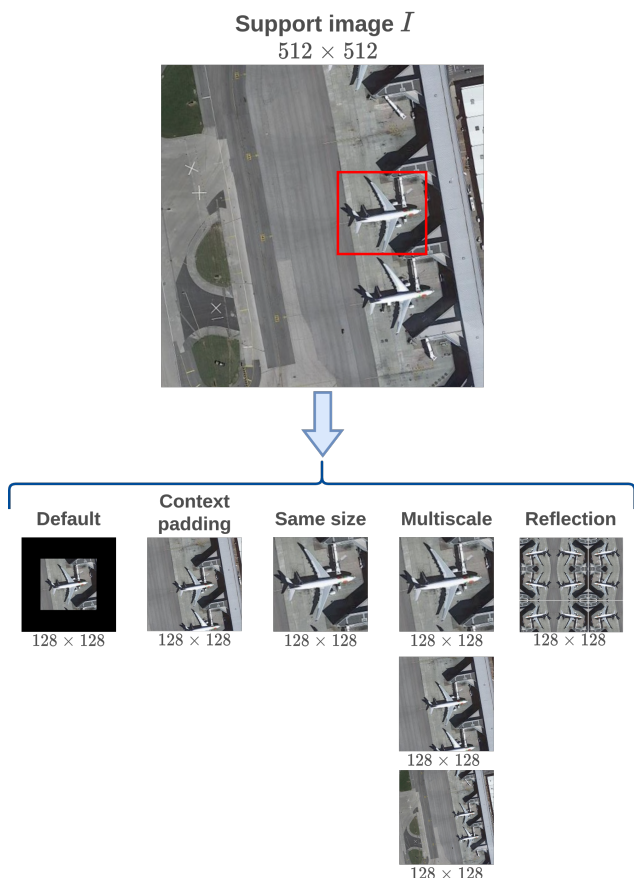


Fig. 9. Illustration of the different cropping strategies tested. The mixed strategy is not illustrated as it is a combination of *default* and *same-size*.

APPENDIX E EVOLUTION OF MAP WITH THE NUMBER OF SHOTS

On Pascal VOC, we conducted an analysis on the influence of the number of shots on the performance. The results

TABLE 9
 $mAP_{0.5}$ values on Pascal VOC for FRW, WSAAN, DANA, MRFCN and DRL as reported in their respective papers. “-” indicates that the value is not reported in the paper.

Method Backbone	FRW [3] Darknet		WSAAN [30]		DANA [37] ResNet50		MRFCN [34] ResNet101		DRL [36]	
	Base	Novel	Base	Novel	Base	Novel	Base	Novel	Base	Novel
# Shots	-	0.148	-	-	-	-	-	0.430	-	0.280
1	-	0.267	-	-	-	-	-	0.606	-	0.494
3	-	0.339	-	-	-	-	-	0.661	-	0.499
5	0.697	0.472	-	-	-	-	-	0.654	-	0.594
10	-	-	-	-	-	-	-	-	-	-

TABLE 10
 $mAP_{0.5:0.95}$ values on MS COCO for FRW, WSAAN, DANA, MRFCN and DRL as reported in their respective papers. “-” indicates that the value is not reported in the paper.

Method Backbone	FRW [3] Darknet		WSAAN [30]		DANA [37] ResNet50		MRFCN [34] ResNet101		DRL [36]	
	Base	Novel	Base	Novel	Base	Novel	Base	Novel	Base	Novel
# Shots	-	0.056	-	-	-	0.186	-	0.127	-	0.109
10	-	0.091	-	-	-	0.216	-	0.166	-	0.15
30	-	-	-	-	-	-	-	-	-	-

are available in Tab. 2, but to better catch the trend, these are represented as plots in Fig. 10. In addition, the same curves are also plotted for each class individually in Fig. 8. These two figures highlight a known trend in few-shot learning: the performance increases with the number of shots. However, this trend is stronger for novel classes. This is expected as the models did not receive heavy supervision for these classes. Interestingly, the trend is less pronounced for novel classes that are really close to some base classes. As an example, the class *cow* belongs to the novel classes set but is visually similar to the classes *sheep* and *horse* from the base set. The mAP for *cow* is high compared to other novel classes and does not benefit as much from having more shots. The models can efficiently adapt their representations of the known classes to match the new one. In Fig. 8, one can notice decreasing performance when the number of shots increases for some classes. This is not surprising, support

examples are sampled randomly and can sometimes be poor representatives of their class, thus misleading the detections. This mostly happens with a small number of shots as the feature averaging reduces the influence of outliers. As an example, performance for the class *car* is reduced for all tested methods between 1 and 3 shots (the support sets are the same for all methods). The magnitude of this loss depends on the method. FRW, WSAAN and DANA are more robust than others to poor examples. The opposite can also occur when the chosen examples are good representatives of their class. As an example, the class *horse* is surprisingly well detected with 3 shots compared with 1 shot.

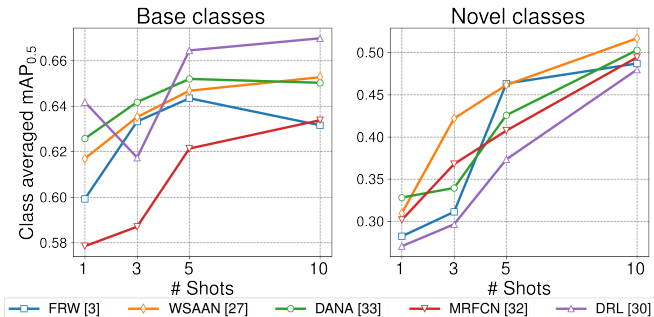


Fig. 10. Evolution of $mAP_{0.5}$ with the number of shots averaged on base and novel classes separately. Each line represents one of the reimplemented methods.

APPENDIX F RELATIVE MAP ANALYSIS ON DOTA, DIOR AND PASCAL VOC

Relative mAP (RmAP), given by Eq. (6), is a reliable measure of how well a FSOD method performs against the classical baseline. However, when the performance of the baseline is poor, small drops in FSOD regime can lead to arbitrary large values of RmAP. While, it is still a valid measurement of the FSOD performance gap, it is not convenient for visualization. One large value will squeeze the others (mostly contained in the band -80% , $+50\%$) and reduce visibility. This is why we chose to only report the mAP difference in Fig. 5. For the sake of clarity, the same results with RmAP are visible in Fig. 11.

We also include in Fig. 12 a plot aggregating the results on the three datasets of interest. This way, the trend line for novel classes is more reliable as it is computed from more data points. In addition, it shows that the trends observed on each dataset are coherent, even between aerial and natural images. It means that the different performance regimes between aerial and natural images are explained only by the size of the objects and not by the different aspects of the objects in the images. Therefore, we could roughly extrapolate the FSOD performance of a given method on other datasets, only provided with the objects' size statistics.

In order to assess how well the XQSA method performs on aerial and natural images, we present in Fig. 13 an extended version of the plot from Fig. 3 with DANA and XQSA. The exact values of mAP and RmAP are regrouped in Tab. 11. This summarizes the conclusions from Sec. 5,

XQSA improves largely over the previous methods on DOTA and DIOR. However, there remains a large performance gap compared to the no few-shot baseline, i.e. the RmAP (white percentage values on the bar chart) is still low compared with RmAP on natural images.

TABLE 11
 $mAP_{0.5}$ and RmAP values for some reimplemented methods and XQSA with $K = 10$ shots. These are the values used to make the plot from Fig. 13

	DOTA		DIOR		Pascal VOC	
	Base	Novel	Base	Novel	Base	Novel
$mAP_{0.5}$						
FCOS baseline	0.61	0.70	0.73	0.82	0.66	0.68
FRW	0.49	0.35	0.61	0.37	0.63	0.49
WSAAN	0.47	0.35	0.63	0.32	0.65	0.52
DANA	0.54	0.37	0.63	0.38	0.65	0.52
XQSA	0.51	0.41	0.60	0.42	0.51	0.47
RmAP (%)						
FRW	-19.43	-49.36	-15.83	-54.23	-3.52	-28.39
WSAAN	-23.24	-49.60	-13.78	-60.26	-0.30	-24.00
DANA	-11.30	-47.63	-13.88	-53.14	-0.46	-23.17
XQSA	-16.03	-41.17	-17.78	-49.05	-21.97	-31.39

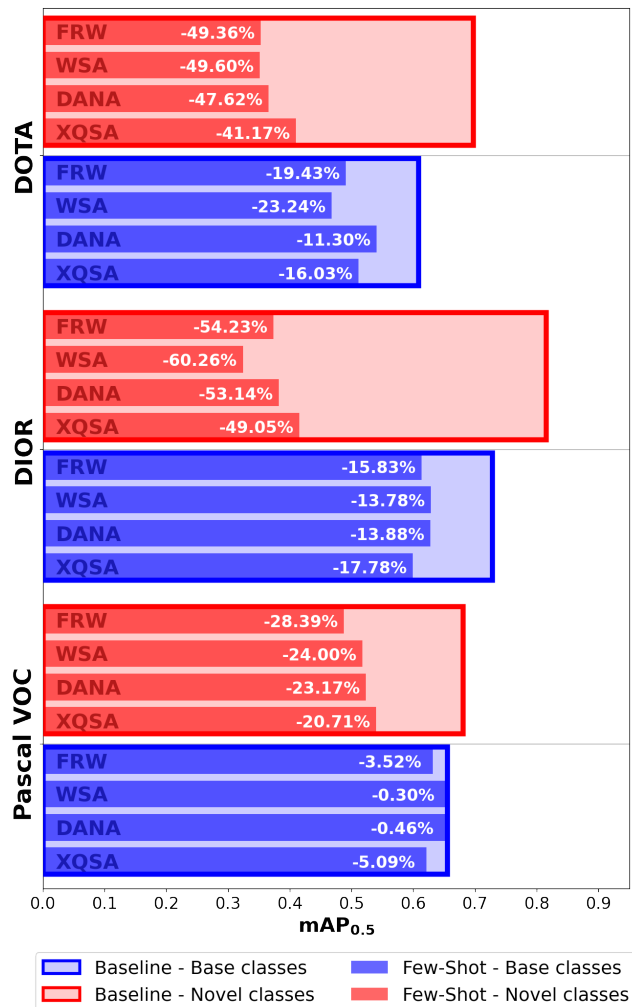


Fig. 13. $mAP_{0.5}$ and corresponding RmAP values of the four best performing methods from all our experiments. All methods are trained within our proposed AAF framework with data augmentation which explains slightly higher performance for FRW and WSA. 10 shots are available for each class at inference time.

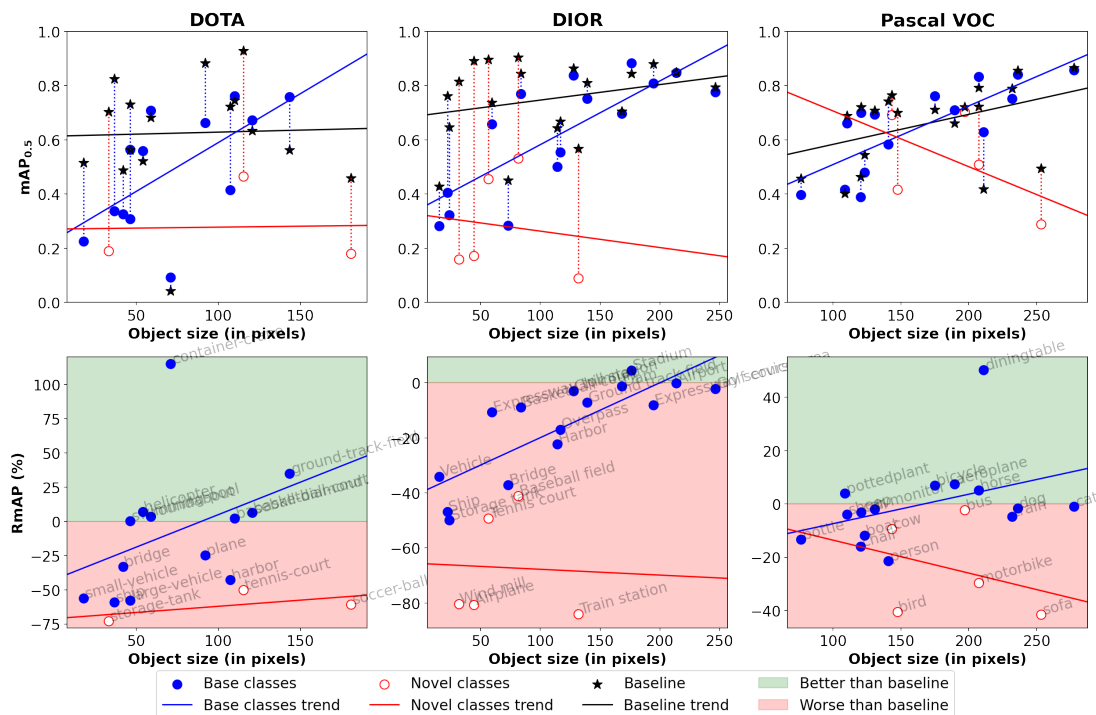


Fig. 11. Comparison of FRW (FSOD) and FCOS (baseline) performance against object size on each dataset separately: DOTA, DIOR and Pascal VOC. **(top)** absolute $mAP_{0.5}$ values. **(bottom)** RmAP computed against the regular baseline (i.e. without few-shot).

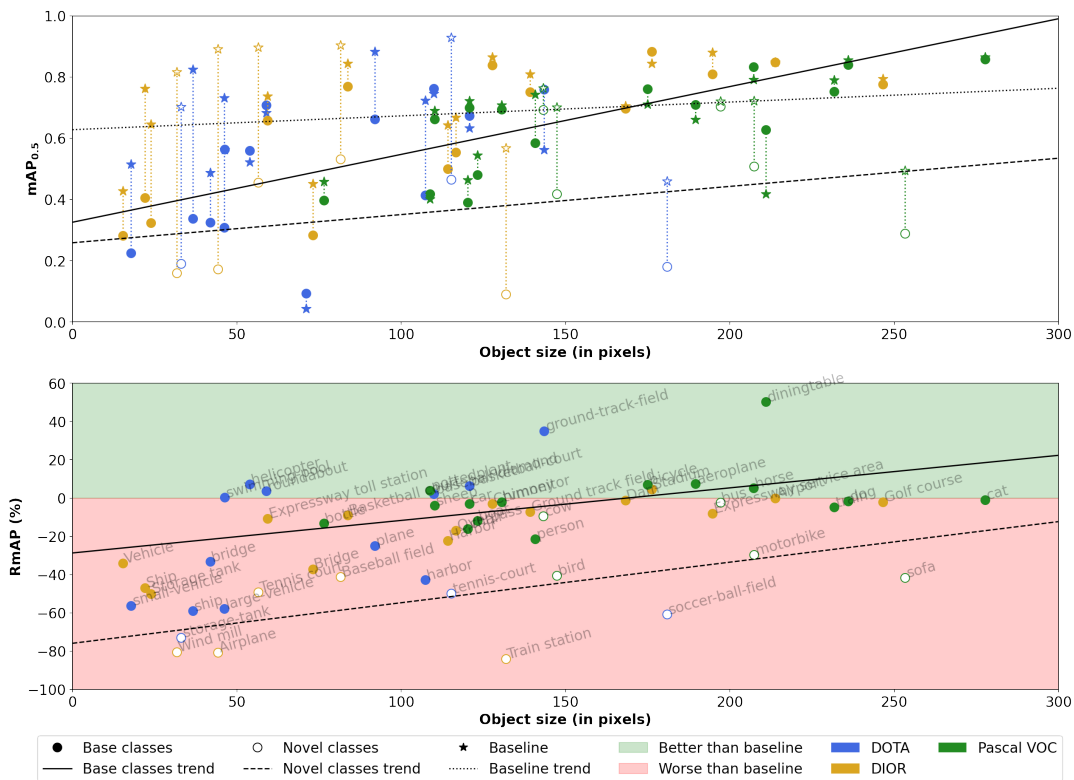


Fig. 12. Comparison of FRW (FSOD) and FCOS (baseline) performance against object size on the three datasets DOTA, DIOR and Pascal VOC together. **(top)** absolute $mAP_{0.5}$ values. **(bottom)** RmAP computed against the regular baseline (i.e. without few-shot).

APPENDIX G

QXSA COMPLEMENTARY RESULTS

In complement for Tab. 5, we also provide the comparison between XQSA, DANA and FRW with $mAP_{0.5:0.95}$ metric and on MS COCO datasets. The results are provided in Tabs. 12 to 16. Results on MS COCO are in agreement with the results on Pascal VOC. XQSA is beneficial especially for novel and small objects. Overall, as MS COCO mostly contains medium and large objects, the performance of XQSA is just barely better than DANA's and FRW's on novel classes. However, on base classes, the performance drops significantly.

$mAP_{0.5:0.95}$ is a more demanding metric for object detection. It is especially hard for small objects as a few pixels shift from ground truth can greatly reduce the IoU and therefore lead to a missed detection. This intensifies as the IoU threshold increases in the mAP computation. For DOTA and DIOR, results with $mAP_{0.5:0.95}$ are in agreement with results from Tab. 5 (i.e. with $mAP_{0.5}$). However, XQSA does not perform better than DANA on Pascal VOC and MS COCO novel classes with $mAP_{0.5:0.95}$. This is mainly due to the metric being too strict on small objects. This questions the soundness of these metrics for FSOD, especially when dealing with small objects.

TABLE 12
Performance comparison between FRW, DANA and XQSA (ours) on DOTA. Reported values are $mAP_{0.5:0.95}$.

mAP _{0.5:0.95} on DOTA								
	Base				Novel			
	All	S	M	L	All	S	M	L
FRW	0.232	0.086	0.278	0.322	0.160	0.042	0.141	0.296
DANA	0.266	0.114	0.307	0.376	0.172	0.056	0.204	0.324
XQSA	0.253	0.089	0.288	0.346	0.210	0.079	0.252	0.265

TABLE 13
Performance comparison between FRW, DANA and XQSA (ours) on DIOR. Reported values are $mAP_{0.5:0.95}$.

mAP _{0.5:0.95} on DIOR								
	Base				Novel			
	All	S	M	L	All	S	M	L
FRW	0.356	0.026	0.230	0.508	0.200	0.005	0.170	0.333
DANA	0.364	0.035	0.249	0.523	0.204	0.008	0.175	0.340
XQSA	0.348	0.035	0.229	0.515	0.228	0.010	0.210	0.348

TABLE 14
Performance comparison between FRW, DANA and XQSA (ours) on Pascal VOC. Reported values are $mAP_{0.5:0.95}$.

mAP _{0.5:0.95} on Pascal VOC								
	Base				Novel			
	All	S	M	L	All	S	M	L
FRW	0.379	0.065	0.228	0.505	0.291	0.056	0.122	0.400
DANA	0.391	0.127	0.064	0.317	0.317	0.052	0.111	0.434
XQSA	0.274	0.032	0.166	0.368	0.251	0.064	0.127	0.352

TABLE 15
Performance comparison between FRW, DANA and XQSA (ours) on MS COCO. Reported values are $mAP_{0.5}$.

mAP _{0.5} on MS COCO								
	Base				Novel			
	All	S	M	L	All	S	M	L
FRW	0.290	0.131	0.359	0.480	0.241	0.115	0.225	0.387
DANA	0.381	0.233	0.518	0.564	0.247	0.120	0.294	0.379
XQSA	0.316	0.161	0.401	0.498	0.250	0.126	0.261	0.385

TABLE 16
Performance comparison between FRW, DANA and XQSA (ours) on MS COCO. Reported values are $mAP_{0.5:0.95}$.

mAP _{0.5:0.95} on MS COCO								
	Base				Novel			
	All	S	M	L	All	S	M	L
FRW	0.156	0.055	0.188	0.278	0.124	0.048	0.109	0.208
DANA	0.225	0.102	0.297	0.365	0.134	0.053	0.150	0.215
XQSA	0.114	0.044	0.142	0.320	0.103	0.049	0.100	0.167

APPENDIX H

QXSA ABLATION STUDY

To confirm the benefits of each component of our attention methods, we conduct a brief ablation experiment, adding separately the different modules of our proposed attention mechanism. The ablation is conducted on DOTA and the results are available in Tab. 17. From this table, it is clear that each component plays a role in the better performance of our method. Both the fusion (with the MLP) and the skip connections around fusion and alignment are beneficial for the performance on novel classes. It is worth to note that Background Attenuation proposed by [37] helps both for base and novel classes, which confirms the experiments conducted by the authors.

TABLE 17
Ablation study of the XQSA attention method on DOTA dataset. Each component is added separately to assess its respective benefits for detection. mAP scores are reported for base and novel classes with $K = 10$ shots.

Multiscale Alignment	✓	✓	✓	✓
MLP Fusion		✓	✓	✓
Skip Connections			✓	✓
Background Attenuation				✓
Base classes	0.492	0.495	0.491	0.511
Novel classes	0.365	0.388	0.403	0.410